Chaotic advection in a cavity flow with rigid particles

Chaotic advection in a cavity flow with rigid particles

Wook Ryol Hwang,[a] Patrick D. Anderson,[b] and Martien A. Hulsen
Materials Technology, Eindhoven University of Technology, P.O. Box 513, 5600MB Eindhoven, The Netherlands

(Received 30 March 2004; accepted 9 February 2005; published online 4 April 2005)

The effect of freely suspended rigid particles on chaotic material transport in a two-dimensional cavity flow is studied. We concentrate on the understanding of the mechanism how the presence of a particle affects the dynamical system of the flow. In contrast to the case studied by Vikhansky ["Chaotic advection of finite-single bodies in a cavity flow," Phys. Fluids **15**, 1830 (2003)], we show that even a regular periodic motion of a single particle can induce chaotic advection around the particle, as a result of the perturbation of the flow introduced by the freely rotating solid particle. This perturbation is of a hyperbolic nature. In fact, stretching and folding of the fluid elements are guaranteed by the occurrence of the hyperbolic flow perturbation centered at the particle and by the rotation of the freely suspended particle, respectively. The fluid-solid flow problem has been solved by a fictitious-domain/finite-element method based on a rigid-ring description of the solid particle. A single-particle system is studied in detail in view of the dynamical systems theory and then extended to two- and three-particle systems. © *2005 American Institute of Physics*.
[DOI: 10.1063/1.1884465]

I. INTRODUCTION

Experiments by Marić and Macosko[1] show that the addition of a small number of balls into a minimixer significantly improves the dispersion characteristics in polymer blends. Their results show that the balls enhance the circulation of materials from low to high shear rate regions and promote breakup of drops.

In this work, we examine the direct influence of the addition of such a ball on distributive mixing. We study chaotic advection of fluids in a simple lid-driven cavity flow containing freely suspended inertialess rigid particles using dynamical systems theory and numerical simulations. A large number of papers are published which deal with the influence of a time-periodic movement of different walls[2,3] on chaotic advection.[4] Other studies show the influence of changes in the geometric aspect ratio of the cavity,[5] while some others show that a single oscillating wall can induce chaotic advection if inertia becomes important.[6]

Vikhansky[7] also studied cavity flows with rigid particles and claimed that the Lagrangian chaos of the particle motion induces Eulerian chaos of the flow. Admittedly, this argument seems evident especially in flows possessing many particles with complicated time-dependent particle movements, because of complex interactions between particle/particle and particle/fluid (referred to Lagrangian chaos of the particle motion in Ref. 7). In this work, however, we report that even a regular periodic motion of a single particle can induce chaotic advection of the fluid material as well. We concentrate on understanding the mechanism how the existence of a particle affects the dynamical systems of the flow, by visualizing dynamical systems structures and related chaotic mixing behavior through the stretching and folding of fluid elements.

As a simple illustration, let us consider a single-particle suspended freely in simple shear flow with shear rate $\dot{\gamma}$, see Fig. 1 with the coordinate system given therein. When the particle is small enough compared to the size of the domain, the angular velocity of the particle equals $-\frac{1}{2}\dot{\gamma}$ (Ref. 8). The velocity field *inside the particle* can be simply expressed in a decoupled form

$$\boldsymbol{u}_p = \boldsymbol{U}_{\mathrm{ssf}} + \boldsymbol{u}', \tag{1}$$

where $\boldsymbol{u}_p = (\frac{1}{2}\dot{\gamma}y, -\frac{1}{2}\dot{\gamma}x)$ is the rigid-body motion of the particle, $\boldsymbol{U}_{\mathrm{ssf}} = (\dot{\gamma}y, 0)$ is the given shear flow in the far field, and $\boldsymbol{u}' = (-\frac{1}{2}\dot{\gamma}y, -\frac{1}{2}\dot{\gamma}x)$ is the perturbed velocity field which appears as a result of the presence of the particle. The $\boldsymbol{U}_{\mathrm{ssf}}$ velocity on the surface of the particle together with the far-field conditions leads to a simple shear flow solution outside the particle. The presence of the particle perturbs the velocity field with the solution that is found by prescribing $\boldsymbol{u}'$ as a boundary condition on the surface of the particle and zero velocity as a far-field condition. The perturbation is hyperbolic: fluid material stretches exponentially in the directions 135° and −45° from the shear direction at the rate $\frac{1}{2}\dot{\gamma}$ and contracts exponentially in the other directions at the same rate. It is most effective in a region surrounding the rigid particle, since on the *surface* of the particle the combined velocity fields generate a rigid-body motion solution and in the far field the perturbation is zero.

In addition, the rotation of the freely suspended particle changes the location of the maximum stretch relative to the particle boundary continuously and, as a result, lead to folding of the elements. This mechanism towards chaos is distinct from that discussed by Vikhansky.[7] He concluded that the flow becomes nonperiodic under the action of the chaoti-

[a]Present address: School of Mechanical and Aerospace Engineering, Gyeongsang National University, Gajwadong 900, Jinju, South Korea.
[b]Author to whom correspondence should be addressed. Electronic mail: p.d.anderson@tue.nl

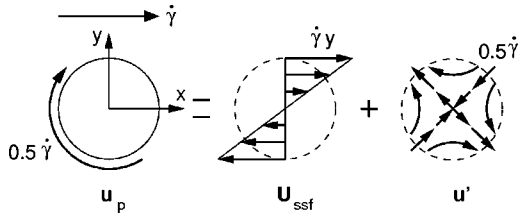

FIG. 1. Decomposition of the velocity field inside the particle for simple shear flow. The hyperbolic perturbed flow $\boldsymbol{u}'$ appears due to the presence of the particle and generates also a hyperbolic perturbed flow outside the particle.

cally advected particles and the force that the particle exerts on the fluid and the geometry of the liquid-filled region evolve in a chaotic manner.

The objective of this work is to understand how the presence of a single particle, and later a small number of particles, affects the dynamics of the flow, and in the end, the mixing performance of the system. Throughout the study, we focus on a simple model flow system: the two-dimensional lid-driven cavity flow in the Stokes regime, which is regular and integrable in the absence of a rigid particle. In order to solve the solid-liquid flow problem computationally, we use a rigid-ring description for the particle, developed by Hwang *et al.*[9]

The paper is organized as follows. First, we describe the system in a mathematical context. Then, in Sec. III, the numerical models are described which are applied to obtain the velocity field. In addition, the front tracking model used in the mixing analysis will be described. In Sec. IV, we discuss single-particle problems: dynamical systems modeling, flow fields/deformation patterns, and the dynamical system structures caused by the addition of the particle. Finally, results are presented for two- and three-particle problems in Sec. V emphasizing general mechanisms which induces chaotic fluid advection.

II. SYSTEM

In this study, we consider freely suspended (i.e., force-free and torque-free) circular disk particles in a Newtonian fluid, in which inertia is neglected for both the fluid and the particles. The two-dimensional lid-driven cavity flow containing these particles is illustrated in Fig. 2. The entire domain Ω, including the interior of the particle, is the computational domain of this work and the four boundaries of Ω are denoted by Γ_i $(i=1,2,3,4)$ and $\Gamma=\cup_{i=1}^{4}\Gamma_i$. The upper boundary Γ_3 is subject to the constant drag velocity $\boldsymbol{u}_D$. The Cartesian x and y coordinates are selected as parallel and normal to the drag velocity direction, respectively. Particles are denoted by $P_i(t)$ $(i=1,\ldots,N)$ and N is the number of particles. We use the symbol $P(t)$ for $\cup_{i=1}^{N}P_i(t)$, the collective region occupied by particles at a certain time t. For a particle P_i, $\boldsymbol{X}_i=(X_i,Y_i)$, $\boldsymbol{U}_i=(U_i,V_i)$, $\boldsymbol{\omega}_i=\omega_i\boldsymbol{k}$, and $\boldsymbol{\Theta}_i=\Theta_i\boldsymbol{k}$ are used for the coordinates of the particle center, the translational velocity, the angular velocity and the angular rotation, respectively; and $\boldsymbol{k}$ is the unit vector in the direction normal to the plane.

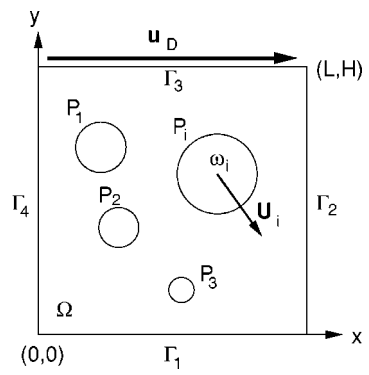

FIG. 2. The lid-driven cavity flow with rigid disk particles.

The set of equations for the fluid domain is given by

$$\boldsymbol{\nabla}\cdot\boldsymbol{\sigma}=\boldsymbol{0} \quad \text{in } \Omega\setminus P(t), \tag{2}$$

$$\boldsymbol{\nabla}\cdot\boldsymbol{u}=0 \quad \text{in } \Omega\setminus P(t), \tag{3}$$

$$\boldsymbol{\sigma}=-p\boldsymbol{I}+2\eta\boldsymbol{D} \quad \text{in } \Omega\setminus P(t), \tag{4}$$

$$\boldsymbol{u}=\boldsymbol{U}_i+\boldsymbol{\omega}_i\times(\boldsymbol{x}-\boldsymbol{X}_i) \quad \text{on } \partial P_i(t) \quad (i=1,\ldots,N), \tag{5}$$

$$\boldsymbol{u}=\boldsymbol{u}_\Gamma \quad \text{on } \Gamma, \tag{6}$$

where $\boldsymbol{u}_\Gamma=\boldsymbol{u}_D$ on Γ_3 and $\boldsymbol{u}_\Gamma=\boldsymbol{0}$ on the other boundaries. Equations (2)–(5) are equations for the momentum balance, the continuity, the constitutive relation, and rigid-body conditions on particle boundaries, respectively. Quantities $\boldsymbol{u}$, $\boldsymbol{\sigma}$, p, $\boldsymbol{I}$, $\boldsymbol{D}$ and η denote the velocity, the stress, the pressure, the identity tensor, the rate of deformation tensor, and the viscosity, respectively. Unknown rigid-body motions in Eq. (5) will be determined by the hydrodynamic interaction. In the absence of inertia, initial conditions are not necessary for the fluid velocity as well as for the particle.

Following the work by Hwang *et al.*,[9] we consider the circular particle as a rigid ring, which is filled with the same fluid as in the fluid domain and the rigid-body condition is imposed on the particle boundary only. This description is possible for the rigid particle, when inertia is negligible. The idea is similar to the original immersed boundary method of Peskin[10] in which the equations for the fluid velocity are solved for both inside and outside of the moving boundary of zero mass. The rigid-ring description requires a discretization only along the particle boundaries and leads to a significant reduction in memory usage. From the rigid-ring description, the set of governing equations for a region occupied by a particle P_i at a certain time t is

$$\boldsymbol{\nabla}\cdot\boldsymbol{\sigma}=\boldsymbol{0} \quad \text{in } P_i(t), \tag{7}$$

$$\boldsymbol{\nabla}\cdot\boldsymbol{u}=0 \quad \text{in } P_i(t), \tag{8}$$

$$\boldsymbol{\sigma}=-p\boldsymbol{I}+2\eta\boldsymbol{D} \quad \text{in } P_i(t), \tag{9}$$

$$\boldsymbol{u}=\boldsymbol{U}_i+\boldsymbol{\omega}_i\times(\boldsymbol{x}-\boldsymbol{X}_i) \quad \text{in } \partial P_i(t). \tag{10}$$

Equations (7)–(10) are the equations for the momentum balance, the continuity, the constitutive relation, and the boundary condition, respectively, which are exactly the same as the

fluid domain equations in Eqs. (2)–(5). The trivial solution of this problem inside a particle is simply the rigid-body motion, applied on the particle boundary extended to the full particle interior,

$$\boldsymbol{u} = \boldsymbol{U}_i + \boldsymbol{\omega}_i \times (\boldsymbol{x} - \boldsymbol{X}_i) \quad \text{in } P_i(t). \tag{11}$$

In addition, the movement of the particle is given by the kinematic equations

$$\frac{d\boldsymbol{X}_i}{dt} = \boldsymbol{U}_i, \quad \boldsymbol{X}_i|_{t=0} = \boldsymbol{X}_{i,0}, \tag{12}$$

$$\frac{d\Theta_i}{dt} = \omega_i, \quad \Theta_i|_{t=0} = \Theta_{i,0}. \tag{13}$$

Equation (13) is completely decoupled from the other equations.

To determine the unknown rigid-body motions $(\boldsymbol{U}_i, \boldsymbol{\omega}_i)$'s of the particles, one needs balance equations for drag forces and torques on particle boundaries. In the absence of inertia and external forces or torques, particles are force-free and torque-free,

$$\boldsymbol{F}_i = \int_{\partial P_i(t)} \boldsymbol{\sigma} \cdot \boldsymbol{n} ds = \boldsymbol{0}, \tag{14}$$

$$\boldsymbol{T}_i = \int_{\partial P_i(t)} (\boldsymbol{x} - \boldsymbol{X}_i) \times (\boldsymbol{\sigma} \cdot \boldsymbol{n}) ds = \boldsymbol{0}, \tag{15}$$

where $\boldsymbol{T}_i = T_i \boldsymbol{k}$ and $\boldsymbol{n}$ is a normal vector on ∂P_i pointing out of the particle $(i = 1, \ldots, N)$. We did not use an artificial particle-particle collision scheme,[11] because the particle overlap and particle/wall collision could be avoided for the multiple-particle problems we studied in this paper by taking a relatively small time step and a sufficiently refined particle boundary discretization.[9]

Finally, we need equations to describe dynamics of the fluid particles. The motion of the fluid particle is considered passive and is determined by the fluid velocity at the fluid particle location, which depends also on the configuration of the rigid particles. The dynamical system is given by the advection equation

$$\frac{d\boldsymbol{x}}{dt} = \boldsymbol{v}(\boldsymbol{x}, t; \boldsymbol{X}_i(t)), \quad \boldsymbol{x}|_{t=0} = \boldsymbol{x}_0 \quad (i = 1, \ldots, N). \tag{16}$$

The map $\boldsymbol{x}(0) \mapsto \boldsymbol{x}(t)$ defines an area- and orientation-preserving Hamiltonian system, since the incompressibility condition holds in the entire domain.

III. NUMERICAL METHODS

A. The velocity field

Following the combined weak formulation of Glowinski *et al.*[11] in which the hydrodynamic force and torque acting on the particle boundary cancel exactly, Hwang *et al.*[9] derived a weak form with the rigid-ring description of the particle in the sliding biperiodic computational domain. The modification of the weak form for the Dirichlet problem is trivial and therefore we present the final weak form without detailed derivation. In the combined weak formulation, the rigid-body constraint is enforced by the constraint equation using a Lagrangian multiplier, defined on the particle boundary. We denote such a Lagrangian multiplier on ∂P_i by $\boldsymbol{\lambda}^{p,i}$,

$$\boldsymbol{\lambda}^{p,i} \in L^2(\partial P_i).$$

The weak form of the present work can be stated as follows.

For a given particle configuration $\boldsymbol{X}_i$ $(i = 1, \ldots, N)$, find $\boldsymbol{u} \in \mathsf{W}$, $p \in L^2(\Omega)$, $\boldsymbol{U}_i \in \mathbb{R}^2$, $\boldsymbol{\omega}_i \in \mathbb{R}$ and $\boldsymbol{\lambda}^{p,i} \in L^2(\partial P_i(t))$ such that

$$-\int_\Omega p \nabla \cdot \boldsymbol{v} dA + \int_\Omega 2\eta \boldsymbol{D}[\boldsymbol{u}] : \boldsymbol{D}[\boldsymbol{v}] dA + \sum_i^N \langle \boldsymbol{\lambda}^{p,i}, \boldsymbol{v} - [\boldsymbol{V}_i + \boldsymbol{\chi}_i \times (\boldsymbol{x} - \boldsymbol{X}_i)] \rangle_{\partial P_i} = 0, \tag{17}$$

$$\int_\Omega q \nabla \cdot \boldsymbol{u} dA = 0, \tag{18}$$

$$\langle \boldsymbol{\mu}^{p,i}, \boldsymbol{u} - [\boldsymbol{U}_i + \boldsymbol{\omega}_i \times (\boldsymbol{x} - \boldsymbol{X}_i)] \rangle_{\partial P_i} = 0 \tag{19}$$

for all $\boldsymbol{v} \in W_0$, $q \in L^2(\Omega)$, $\boldsymbol{V}_i \in \mathbb{R}^2$, $\boldsymbol{\chi}_i \in \mathbb{R}$, and $\boldsymbol{\mu}^{p,i} \in L^2(\partial P_i(t))$. The function space W and W_0 are the solution and variational space for the velocity, respectively,

$$W = \{H^1(\Omega)^2 | \boldsymbol{u} = \boldsymbol{u}_\Gamma \text{ on } \Gamma\},$$

$$W_0 = \{H^1(\Omega)^2 | \boldsymbol{u} = \boldsymbol{0} \text{ on } \Gamma\},$$

and the inner product $\langle \cdot, \cdot \rangle_{\partial P}$ is the standard inner product in $L^2(\partial P)$,

$$\langle \boldsymbol{\mu}, \boldsymbol{v} \rangle_{\partial P} = \int_{\partial P} \boldsymbol{\mu} \cdot \boldsymbol{v} ds.$$

In this problem, the pressure inside the rigid-ring particle is an undetermined constant. The numerical method with the fictitious domain technique is nonsingular and it chooses a value for the pressure, however, the pressure inside the rigid ring does not affect other results outside the particle. One can even recover the stresslet on the particle boundary using the pressure inside the ring and the Lagrangian multiplier $\boldsymbol{\lambda}^p$ (see Ref. 9).

A regular rectangular discretization is employed for the entire computational domain with biquadratic interpolation of the velocity and linear discontinuous interpolation of the pressure.[9] A discontinuous interpolation of the pressure appears to be mandatory, since an arbitrary location of the particle boundary induces discontinuity in the pressure.[12] The point collocation method has been used for equations for the rigid-ring constraint in Eqs. (17) and (19), e.g.,

$$\langle \boldsymbol{\mu}^{p,i}(\boldsymbol{x}), \boldsymbol{u}(\boldsymbol{x}) - [\boldsymbol{U}_i + \boldsymbol{\omega}_i \times (\boldsymbol{x} - \boldsymbol{X}_i)] \rangle_{\partial P_i} \approx \sum_{k=1}^{M_i} \boldsymbol{\mu}_k^{p,i} \cdot \{\boldsymbol{u}(\boldsymbol{x}_k) - [\boldsymbol{U}_i + \boldsymbol{\omega}_i \times (\boldsymbol{x}_k - \boldsymbol{X}_i)]\}, \tag{20}$$

where M_i, $\boldsymbol{x}_k$, and $\boldsymbol{\mu}_k^{p,i}$ are the number of collocation points on ∂P_i, the position of the kth collocation point, and the multiplier at the collocation point, respectively. We define

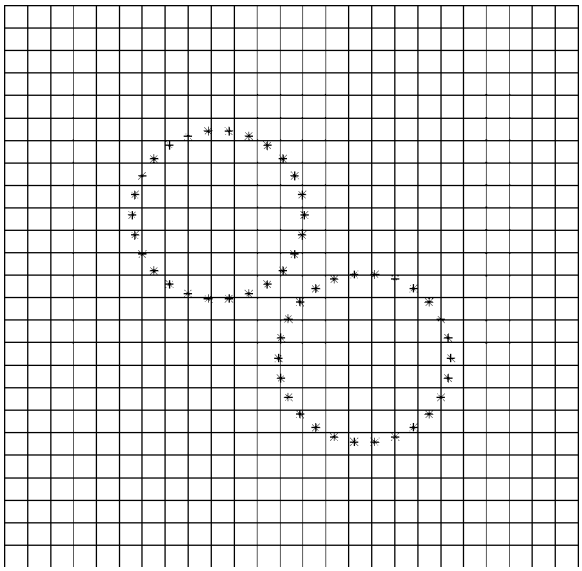

FIG. 3. A regular rectangular discretization is used for the entire computational domain and the particle is described by collocation points along the particle boundary (rigid-ring description).

uniformly distributed collocation points on the particle boundary and the number of collocation points is chosen proportional to the particle radius. An excessively large number of collocation points causes element locking, while too small number of points cannot represent the rigid-body motion of the circular particle accurately. Approximately one collocation point in an element appears to give the most accurate result.[9] (See Fig. 3 for an illustrative example for discretizations for fluid and particles.)

An equation with a sparse symmetric matrix with many zeros on the diagonal appears as a result of the above discretizations, which has been solved by a direct method based on the sparse multifrontal variant of the Gaussian elimination (HSL2002/MA41) for each time step.[9,13] Once the rigid-body velocity of the particle is obtained as a part of the solution, the particle configuration for the next time step is calculated by integrating the kinematic equations [Eqs. (12) and (13)], for which we used an explicit method, the second-order Adams–Bashforth method.

B. Particle tracking

To study the mixing performance in the two-dimensional lid-driven cavity flow an adaptive front tracking model is applied.[14] Initially, only a relatively small amount of markers are required to describe the boundary of the domain to be tracked in time. During the course of tracking nodes are inserted in between nodes where either the distance d has grown beyond a certain limit, or when the angle α_i formed by two consecutive edges is smaller than a critical one α_c, according to the following criteria:

$$d < h, \tag{21}$$

$$d < h_c \quad \text{if } \alpha_i < \alpha_c \vee \alpha_{i-1} < \alpha_c, \tag{22}$$

with

$$d = \|\boldsymbol{x}_{i-1} - \boldsymbol{x}_i\|, \tag{23}$$

$$\alpha_i = \arccos\left(\frac{(\boldsymbol{x}_{i-1} - \boldsymbol{x}_i) \cdot (\boldsymbol{x}_{i+1} - \boldsymbol{x}_i)}{\|\boldsymbol{x}_{i-1} - \boldsymbol{x}_i\| \|\boldsymbol{x}_{i+1} - \boldsymbol{x}_i\|} \right), \tag{24}$$

where h and h_c are the maximum lengths in straight and curved regions of the boundary, respectively. In case Eqs. (21) and (22) are not satisfied, the edge between $\boldsymbol{x}_{i-1}$ and $\boldsymbol{x}_i$ is split into two parts and a new node is inserted at an earlier time level and tracked to the current time. The actual tracking of the individual markers requires the solution of the ordinary differential equation (16), which is performed using an adaptive fourth-fifth order Runge–Kutta scheme.

IV. SINGLE-PARTICLE PROBLEMS

We begin with the simplest case: a single rigid particle, initially at the center of the cavity, in the lid-driven cavity flow. To make the problem more tractable in the view of the classical dynamical systems diagnostics, we consider only the case when the orbit of the rigid particle is sufficiently far apart from the wall such that complicated particle-wall interactions can be neglected. In this case, the motion of the rigid particle appears to be periodic in time (i.e., it returns back to the original position) and the velocity field of the fluid becomes time periodic as well.

A. Modeling

We define the period T as the time it takes for the rigid particle to return to its original position; the period only depends on the initial location and the size of the particle. In this specific problem, we prefer to use a phase variable ϕ rather than t,

$$\phi = \omega t, \quad \mathrm{mod}(2\pi), \quad \phi \in S, \tag{25}$$

where $\omega = 2\pi/T$ and S is a circle of period 2π. We are now able to rewrite the dynamical system [Eq. (16)] in the extended phase space $\mathbb{R}^2 \times S$,

$$\dot{x} = u(\boldsymbol{x}; \boldsymbol{X}(\phi)), \quad \dot{y} = v(\boldsymbol{x}; \boldsymbol{X}(\phi)), \quad \dot{\phi} = \omega. \tag{26}$$

Since the flow is periodic in time, the Poincaré map can be naturally selected as a two-dimensional map from one xy plane to the next periodic xy plane along the flow in the extended space. In the extended space, the physical xy plane at ϕ_0 can be identified as the cross section Σ_{ϕ_0},

$$\Sigma_{\phi_0} = \{(x, y, \phi) | \phi = \phi_0 \in [0, 2\pi]\}.$$

Then the Poincaré map of Σ_{ϕ_0} into Σ_{ϕ_0} is defined as

$$P_{\phi_0}: \Sigma_{\phi_0} \to \Sigma_{\phi_0}, \quad \boldsymbol{x}(\phi_0/\omega) \mapsto \boldsymbol{x}((2\pi + \phi_0)/\omega). \tag{27}$$

The map preserves the area and the orientation. Now consider the symmetry in the Poincaré map. The motion of a single particle in the cavity flow is depicted in Fig. 4 in the

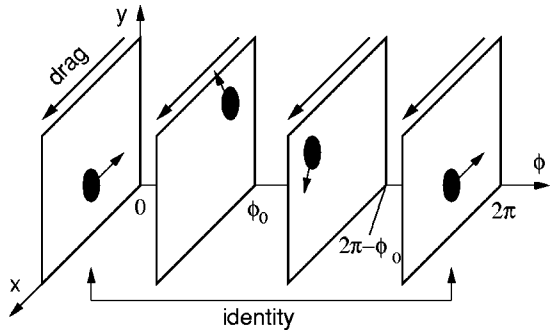

FIG. 4. The motion of a single rigid particle in a lid-driven cavity flow in an extended phase space.

extended phase space. By inspection, one can get the symmetry of the velocity field $\boldsymbol{u}$,

$$u(x,y,\phi) = u(1-x,y,2\pi-\phi),$$
$$v(x,y,\phi) = -v(1-x,y,2\pi-\phi). \tag{28}$$

Using the reflection symmetry about $x=1/2$,

$$S:(x,y) \to (1-x,y), \tag{29}$$

one can obtain the symmetry in the Poincaré map from Eq. (28) as follows:

$$P_{2\pi-\phi_0}^{-n} = SP_{\phi_0}^{n}S, \tag{30}$$

where $P_{\phi_0}^{n}$ is the nth iterate of P_{ϕ_0} and $P_{\phi_0}^{-n}$ is the inverse of $P_{\phi_0}^{n}$. See the Appendix for the derivation and more detailed procedures for similar problems that can be found in Hwang *et al.*[15,16] From Eq. (30), Poincaré sections defined at $\phi=0$ and π satisfy the reflection symmetry about $x=1/2$ by themselves.

B. The flow field and deformation patterns

Throughout this work, we use the square cavity as shown in Fig. 2 with $L=H=1$ as the computational domain and the upper drag velocity and the viscosity are given $u_D=1$ and $\eta=1$, respectively. The first test case is constructed as follows: a single particle with radius $r=0.075$ is initially suspended at (0.5, 0.5), the center of the domain. We used a 100×100 mesh for the computation with 48 collocation points for the particle and a time step of 0.01. A 100×100 mesh provides an accurate solution for the velocity and the velocity gradient.[9] The front tracking is performed to obtain the deformation pattern of material (passive) blobs with a fourth-fifth order Runge–Kutta method with an error tolerance of 10^{-7}. During all computations presented in this work the following criteria were applied for the front tracking: $h=0.02$, $h_c=0.01$, and $\alpha_c=140$.

Figure 5 shows the velocity and the location of the rigid particle, which indicates a periodic particle motion with $T=5.71$. Plotted in Fig. 6 are the consecutive deformation patterns of the initially circular material line (the solid line) surrounding the rigid particle (the dotted line) during six periods of flow, with a time interval of $1.2T$. The periodic particle orbit is indicated by the dashed line in the initial

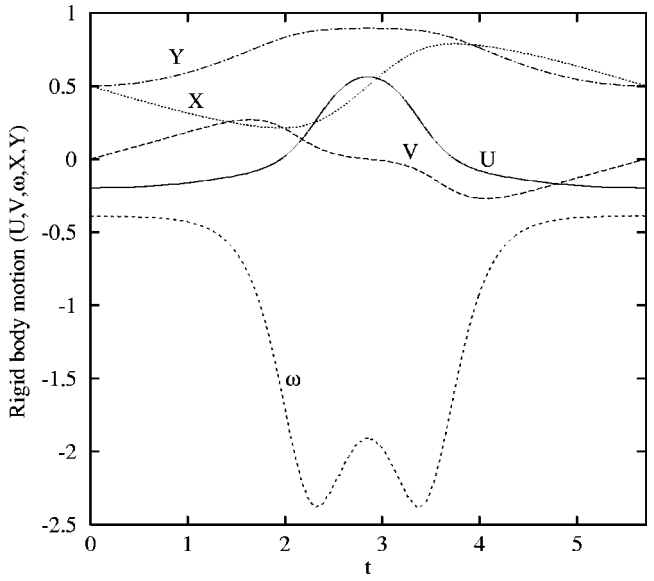

FIG. 5. The particle motion (U,V,ω) and the location (X,Y) of the single-particle problem $(r=0.075)$. The particle motion is periodic with $T=5.71$.

figure (at $t=0$). The length of the closed material line l is also indicated. During front tracking, the enclosed area was kept within 1% variation. The enclosed area is computed along the curve by $(\oint \boldsymbol{x}\cdot\boldsymbol{n}_c ds)/2$, with the outward normal vector $\boldsymbol{n}_c$ along the curve.[17]

The deformation patterns in Fig. 6 show the typical chaotic behavior with stretching/folding and exponential growth of the material line, even though the motion of the rigid particle is regular and periodic (as is the velocity field). There are two stretching directions around the particle boundary in each subpart of Fig. 6 and the direction of the stretch changes in time, due to change of the surrounding velocity field of the particle.

The existence of the two stretching directions is closely related to the perturbed hyperbolic velocity field, as mentioned in the Introduction. To show the effect on the velocity field, we plotted two sets of streamlines at $t=0$: one from the full velocity field $\boldsymbol{u}$ [Fig. 7(a)] and the other [Fig. 7(b)] of the perturbed velocity field $\boldsymbol{u}'=\boldsymbol{u}-\boldsymbol{u}_0$, where $\boldsymbol{u}_0$ is the velocity field in the cavity *without* the particle. In case of the freely suspended particle, there is no significant change in the streamlines with the full velocity field. However, the streamlines of the perturbed velocity field $\boldsymbol{u}'$ show a hyperbolic flow resulting from the presence of the particle. In Fig. 7(b), the stretching of material occurs in two directions, to the right-lower direction and to the left-upper direction around the particle. Compare Fig. 7(b) with the deformation patterns on the particle boundary at $t=6T$ in Fig. 6; also compare it with Fig. 1. The direction of the stretch changes as the particle moves to other positions where the surrounding velocity field is different. In addition, the particle rotates at an angular velocity related to the local vorticity, which leads to the folding of the stretched material lines near the rigid particle. Remark that in simple shear flow the perturbation of the velocity field caused by a rigid particle will not lead to chaotic advection. Without loss of generality we can assume that the particle only rotates and that the velocity is steady. For

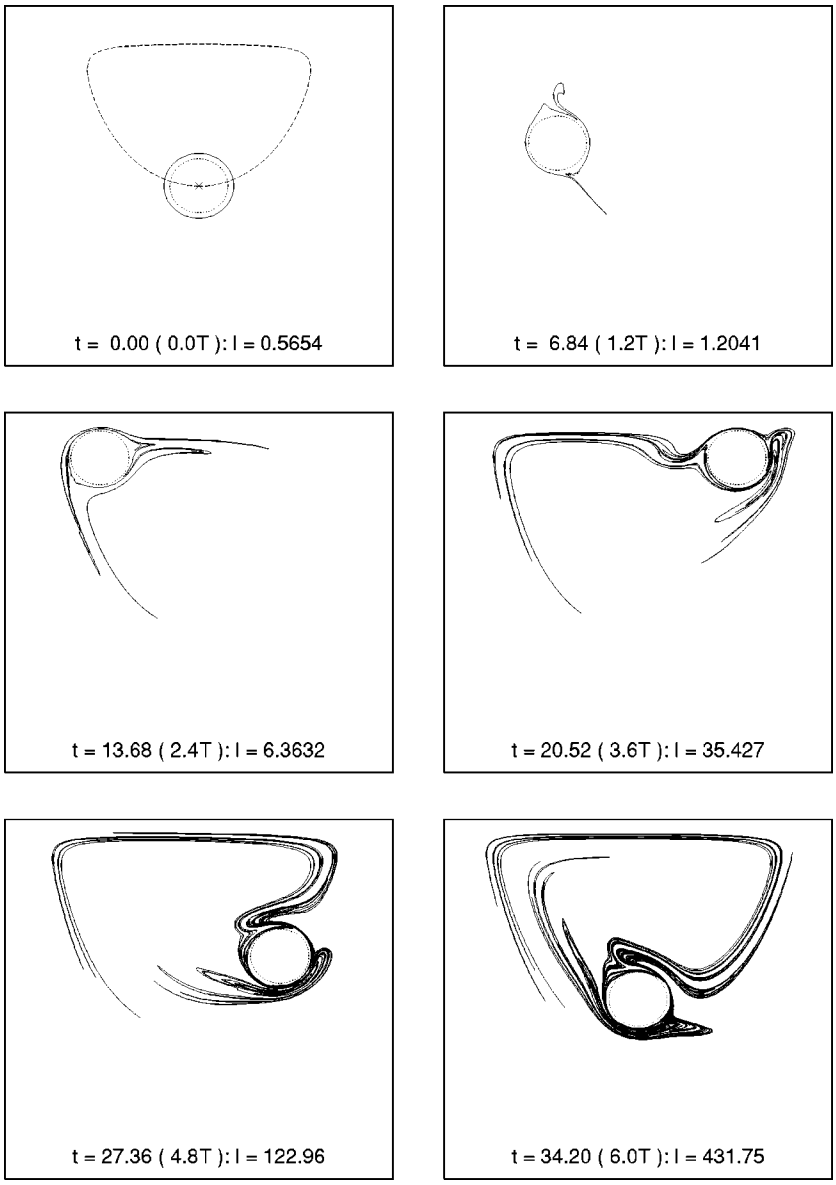

FIG. 6. The deformation patterns of the circular closed material line (solid) surrounding the rigid particle (dotted) for six periods in time. The length of the closed material line l is also indicated. The radius of the particle is $r=0.075$ and the initial location is (0.5,0.5). The dashed curve in the initial figure ($t=0$) indicates the particle orbit.

steady two-dimensional flows it is well known that chaotic mixing is not possible.[3,4]

C. Dynamical systems

The Poincaré sections at three different phases, $\phi=0$, $2\pi/3$, and π, are presented for the single-particle problem with $r=0.075$ in Fig. 8 in order to visualize the dynamical structure in the extended space. A set of 400 evenly distributed initial points is integrated in time for 250 periods and then the symmetry relation in Eq. (30) has been applied to obtain the Poincaré sections. The Poincaré sections at $\phi=0$ and π have reflectional symmetry about $x=1/2$; the sections at $\phi=2\pi/3$ and at $4\pi/3$ are symmetric to each other about $x=1/2$.

Figure 8 shows that the dynamical systems in the cavity are partly chaotic and partly regular. Especially, the region around the particle is chaotic, since the region undergoes stretching and folding repeatedly, as mentioned earlier. Interestingly, there is a large Kolmogorov–Arnold–Moser (KAM) torus in the opposite side of the rigid particle. Since it always appears on the opposite side of the particle, we denote this as *the mirrored crescent* and it behaves like a period-1 resonance band. In fact, the mechanism for the creation of the mirrored structure is quite similar to that of the period-1 resonance. We illustrate the mechanism in Fig. 9. Since the particle itself plays the role of a (traveling) hyperbolic fixed point, a corresponding elliptic fixed point should exist inside the region enclosed by the perturbed stable/unstable manifolds connected to/from the hyperbolic fixed point. The largest stable orbit covering the elliptic point defines the region occupied by the mirrored crescent.

The size of the mirrored crescent varies with the size of the rigid particle. The Poincaré sections for $r=0.05$ and 0.1 are presented in Fig. 10 at $\phi=0$. We used the same initial particle position as $r=0.075$ for these two problems. In comparison with Fig. 8 of the same phase, one can see that the mirrored structure increases with the size of the particle. The larger the particle, the larger the region of the superimposed

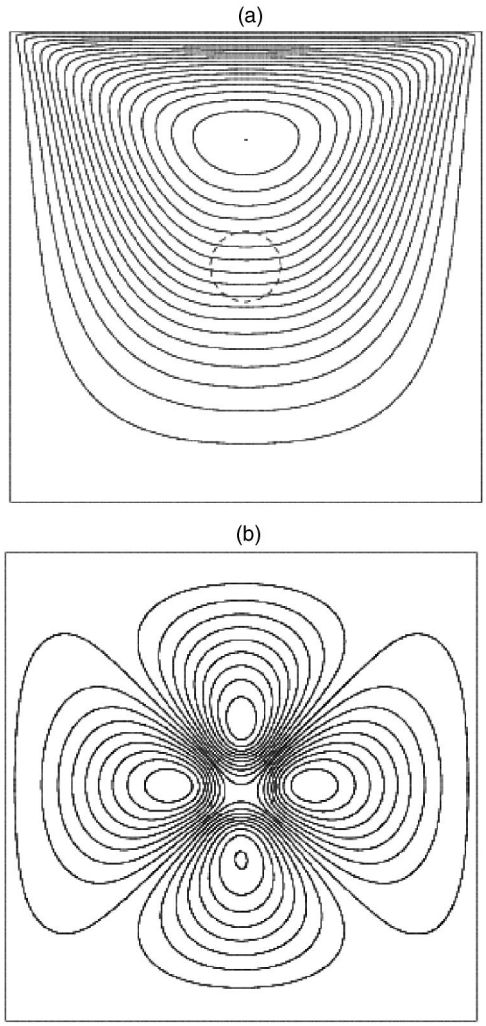

FIG. 7. The streamlines of the single-particle problem ($r=0.075$) at $t=0$: (a) using the full velocity field $\boldsymbol{u}$; (b) using the perturbed velocity field $\boldsymbol{u}'=\boldsymbol{u}-\boldsymbol{u}_0$. $\boldsymbol{u}_0$ is the velocity field of the cavity flow without the particle. The rigid particle is described by the dashed line and is located at (0.5,0.5).

hyperbolic flow, which means that there is a larger region enclosed by the perturbed stable/unstable manifolds connected to/from the hyperbolic fixed point and that the mirrored crescent gets larger as well.

In addition, there are many resonance bands in the Poincaré sections in Figs. 8 and 10. The dynamics of the resonance can be approximately determined by the frequency ratio, denoted by Λ, the ratio of the frequency associated with the fluid rotation f_f in the unperturbed (no-particle) system to the frequency associated with the rigid particle motion f_p. In the single-particle problem, the frequency ratio can be expressed as

$$\Lambda(\zeta)=\frac{f_f(\zeta)}{f_p}=\frac{T_p}{T_f(\zeta)}, \tag{31}$$

where ζ is an index of the orbit of the fluid particle, T_p is the time period of the particle motion, and T_f is the time period of the fluid particle defined in the unperturbed system. Physically the frequency ratio Λ indicates that the number of rotations of the fluid particle during one-particle rotation. We simply take the initial fluid particle y position on the centerline ($x=0.5$) as the index of the orbit ζ. Then the distribution of the frequency ratio is plotted as a function of the initial position y in Fig. 11. The time period of the particle rotation T_p is found to be 5.62 and 5.84 for $r=0.05$ and 0.1, respectively. The dominant rational frequency ratios, possessing a relatively small denominator, are indicated in Fig. 11. In the most weakly perturbed case, $r=0.05$ in Fig. 10(a), one can observe the period-4 ($\Lambda=1/4$), 3 (1/3), 5 (2/5), 2 (1/2), 3 (2/3), 4 (3/4), and 4 (5/4) resonance bands along the centerline ($x=0.5$) from the bottom, which are expected from the frequency ratio distribution. When $r=0.075$, the size of the inner elliptic island of $\Lambda=5/4$ is reduced significantly and the elliptic island of $\Lambda=3/4$ disappears. See $\phi=0$ in Fig. 8 for a direct comparison. In the most perturbed case, $r=0.1$ [Fig. 10(b)], the period-4 ($\Lambda=1/4$) and 5 ($\Lambda=2/5$) have disappeared, due to the increased perturbation. The innermost elliptic rotation has been further destroyed and the period-4 resonance band appeared instead.

To summarize, as the particle size increases, we get a stronger chaotic behavior in the regions governed by the usual resonance phenomena, but at the same time the largest elliptic island of the mirrored crescent increases also. A possibility avoiding the dilemma is to add another rigid particle, which will be discussed in the following section.

Before closing the present section, we show the deformation patterns of small material blobs, originally located around the four elliptic and four hyperbolic fixed points of the period-4 orbit ($\Lambda=5/4$) for $r=0.075$. The location of the first and fourth-order periodic points is determined using a technique similar as presented by Anderson *et al.*[6] We computed the deformation patterns for the 24 periods, since motions in the resonance band are subharmonic and slow (Fig. 12). The patterns show material transports due to the heteroclinic tangles between the neighboring hyperbolic fixed points.

V. PROBLEMS WITH MORE THAN ONE PARTICLE

A. Two-particle problem

Now we proceed to the system possessing two particles. The two-particle problem is constructed carefully such that the motion of the two rigid particles is periodic in time, both with the same period, and thereby the velocity field becomes also periodic. We use two identical particles with radius $r=0.075$. The first particle is again positioned at the center of the cavity (0.5, 0.5), and the second particle position y along the centerline ($x=0.5$) is determined using the Newton–Raphson method to satisfy the periodicity. The location of the second particle was found (0.5, 0.89178). The period during which a particle returns back to its original position corresponds to twice of the period of the two-particle problem, since the two circular particles are identical. In this regard, in the two-particle problem, the period T is defined such that a particle returns to the original position of the other particle, and has been found $T=2.805$ with a 100×100 mesh and a time step of 0.01. With the period T, one can construct the Poincaré map along with its symmetry relation in the same as done for the single-particle problem.

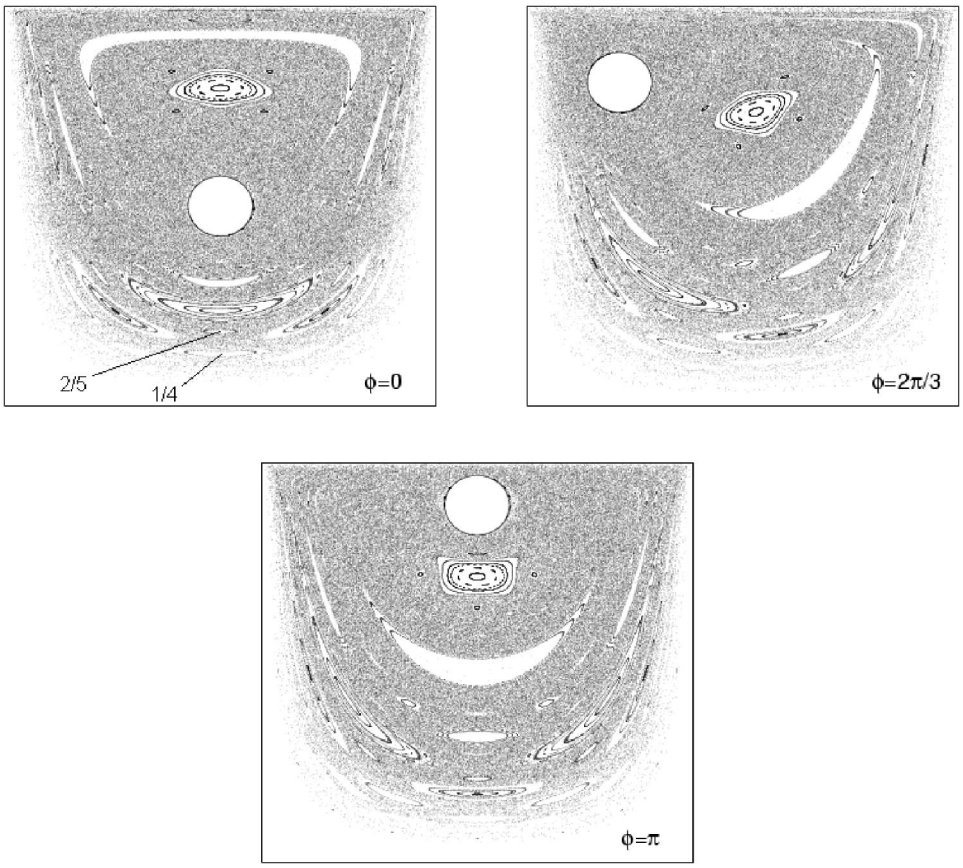

FIG. 8. The Poincaré sections at $\phi=0$, $2\pi/3$, and π for the single-particle problem with $r=0.075$.

Figure 13 shows the Poincaré section of the two-particle problem at $\phi=0$. Unlike the previous single-particle problems, there is no large elliptic island in the opposite side of the particle, since the other particle (or the traveling hyperbolic fixed point) is located exactly where the island would be expected to be present. Although the problem is specially constructed (for the purpose to obtain a periodic flow), one can expect that the destruction (or at least shrinkage) of the mirrored island will take place in general for those problems with more than one particle.

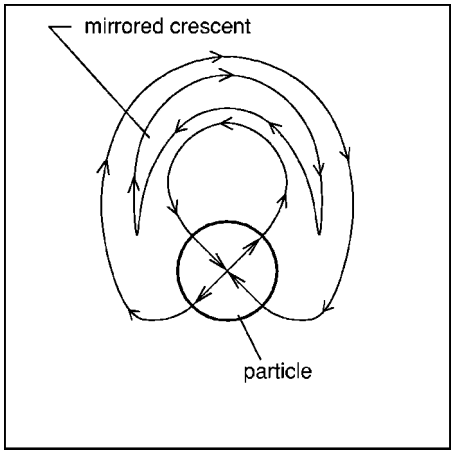

FIG. 9. The occurence of a large KAM torus (the mirrored crescent) in the opposite position of the rigid particle.

There are a number of resonance bands and KAM tori in the Poincaré section (Fig. 13). The resonance bands of period 3, 4, and 5 appear as expected from the frequency ratios $1/3$, $1/4$, and $1/5$ (and $2/5$) in Fig. 11. Note that the period is approximately half the period of the single-particle problems. In Fig. 14 we present six consecutive deformation patterns of a circular fluid blob for 28 periods with an interval of $5.6T$ along with the length stretch l.

Other combinations of two-particle systems can be considered where the ratio of the radii of the two particles may act as a parameter. However, we do not expect any fundamental changes with respect to the dynamics of the mixing flows compared to the case as presented in this paper, and such an analysis is therefore not within the scope of this paper.

B. Three-particle problem

The final example is the system containing three rigid particles of the same size $r=0.05$. There is no periodicity in the flow; at least we could not determine three-particle locations such that the three particles return to their original location after a certain time. We have placed the particles initially at the locations (0.5, 0.4), (0.5, 0.6), and (0.5, 0.8) in the cavity and analyzed the displacement and deformation of a fourth passive blob. The continuous deformation patterns of the initial blob at $t=0$ (initial), 30, 60, and 84 are plotted in Fig. 15. Once again, one can observe the stretching in two directions around the particle boundary.

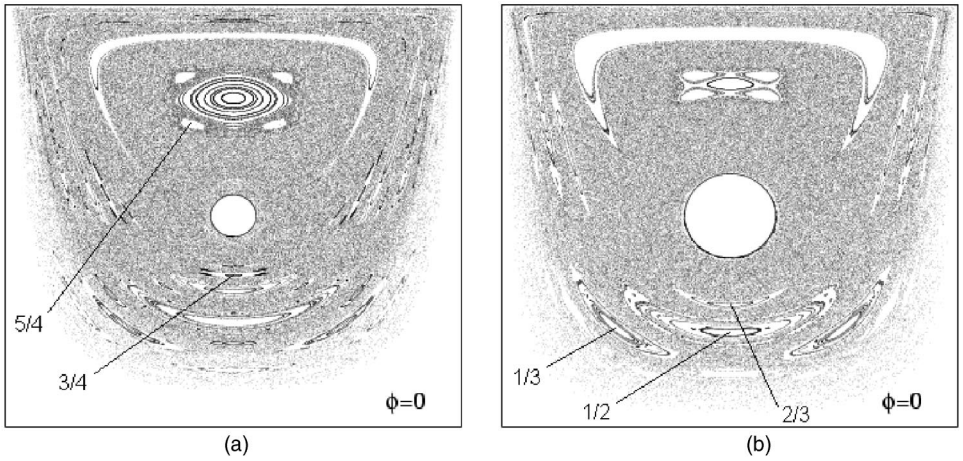

FIG. 10. The Poincaré sections at $\phi=0$ for different rigid particle sizes: (a) $r=0.05$; (b) $r=0.1$.

The particle, initially placed at the lowest position, rotates around the other two particles and the inserted fluid blob. The two other particles continuously tumble while the inserted blob starts to stretch and fold around these two particles. Until $t=46$, the initial lowest particle is not directly involved in the stretching and folding process of the inserted blob. After this time, the blob reaches the lowest particle where it starts to fold around.

In Fig. 16, the length stretch of the circular blob in the three-particle problem is plotted in time and shows the exponential growth confirming that the flow is chaotic. In the same figure results for the single- and two-particle case have been inserted where the length stretch has been scaled with its original length. In order to have a systematic comparison, for the single-particle results, we plotted the result from the initial blob of $r=0.09$ as shown in Fig. 6 and also the initial blob of $r=0.05$ used in the two-particle or three-particle problem using the same location of the blob. The latter one is denoted with the asterisk (∗). For the two-particle problem, the length stretch result using the initial blob of $r=0.05$ as in Fig. 14 along with the two blobs of $r=0.09$ which enclose the upper and the lower particles initially, respectively. In the latter case, the relative length stretch result from the blob embracing the lower particle is denoted with a single asterisk (∗) and the one from the upper particle is denoted with two asterisks (∗∗).

What we clearly see from Fig. 14 is that the stretching and folding really takes place close to the rigid particles, especially in the result for the single-particle case. In the single-particle case we observe the time period of the flow from the length stretch in Fig. 16. Until about $t=5.7$ we see a steady increase in the length stretch, which decreases for a short time, approximately a quarter of a period, and then increases again. Apparently, the flow inhibits regions where contraction takes place for a certain time. After the contraction a steep increase in length stretch is observed again. The process is repeated for every period of flow.

In general, the cases with blobs enclosing the rigid particle show more pronounced length stretch, as one expects from the chaotic region formed near the rigid particle boundary. The results from the two- and three-particle systems with blobs not enclosing the particle in Fig. 16 show that the length stretch is less compared to the single-particle case.

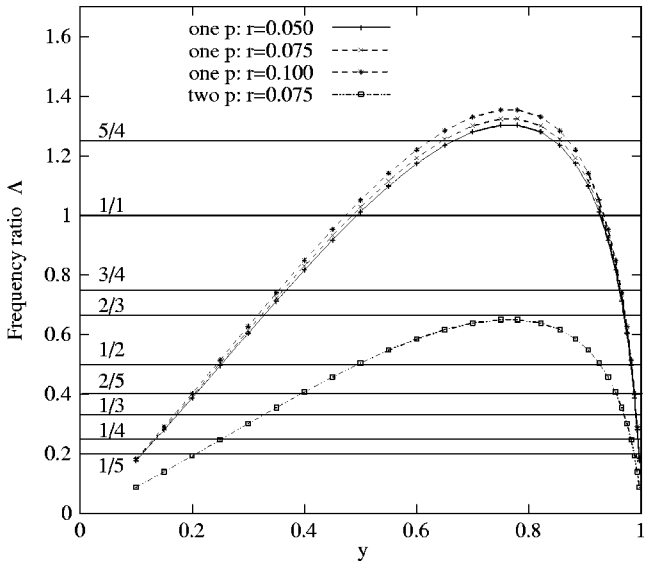

FIG. 11. The frequency ratio distribution of the single- and two-particle problems.

VI. CONCLUSIONS

In this study, we investigated chaotic material advection in a two-dimensional lid-driven cavity flow laden with freely suspended rigid particles, which is regular and integrable in the absence of the particle. We focused on understanding the mechanism how the presence of rigid particles affect the dynamical systems of the flow and lead to chaotic advection. We used a finite-element/fictitious-domain method with a rigid-ring description for the particle to solve the solid-liquid flow and a high-order adaptive frontal tracking method for fluid particle tracking.

In the single-particle problem, which is carefully constructed to keep the flow periodic, we discussed (i) the stretching and folding of fluid material around the particle, (ii) the existence of a large elliptic island (the mirrored crescent) in the opposite side of the particle, which grows with the size of the rigid particle, and (iii) the usual resonance structures which decays with increasing particle size. The reason for these phenomena is the occurrence of hyperbolic

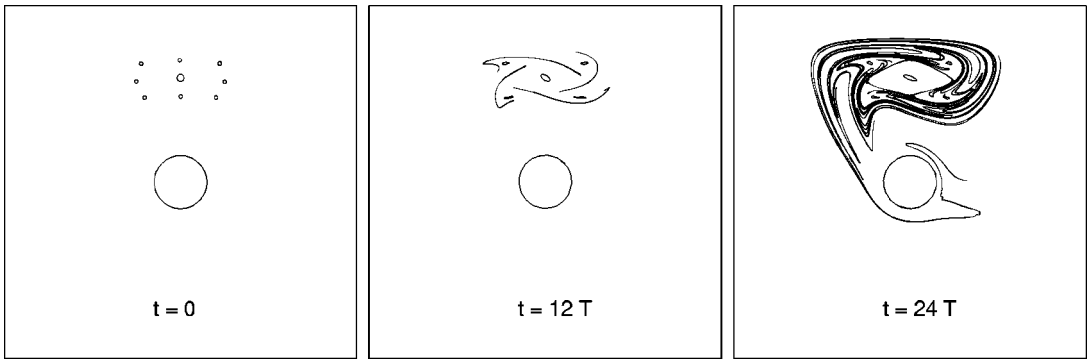

FIG. 12. The consecutive deformation patterns for small material blobs initially located around the four elliptic and hyperbolic fixed points in the orbit of period 4 ($\Lambda=5/4$) in the single-particle problem with $r=0.075$.

perturbed flow caused by the presence of the rigid particle. The two-particle problem is also carefully constructed to satisfy the periodicity. Since one particle has been placed exactly where a mirrored island from the other particle would appear, there does not appear a large mirrored island in the two-particle problem. The single- and two-particle problems are just periodic and there is no Lagrangian chaos in the particle motion, which is a major difference from the work of Vikhansky.[7] The route to chaos in particle-laden flow considered in these problems is not generated by chaotic Lagrangian motion of the particle, but originates from the presence of the freely suspended particles inducing a hyperbolic perturbed flow. We also show results for a three-particle problem, which is not periodic, and discussed mixing patterns along with the length stretch.

The method for solving the solid-fluid problem in this paper can be extended to systems with a viscoelastic fluid, which are of great importance for mixing in polymer processing. In the viscoelastic system, the particle motion, the rheological behavior, and the particle/particle interaction behavior are quite different from Newtonian behavior, e.g., separating two particles generate strong elongational flows between the two particles, which of course affect dynamical systems and mixing performances.[18]

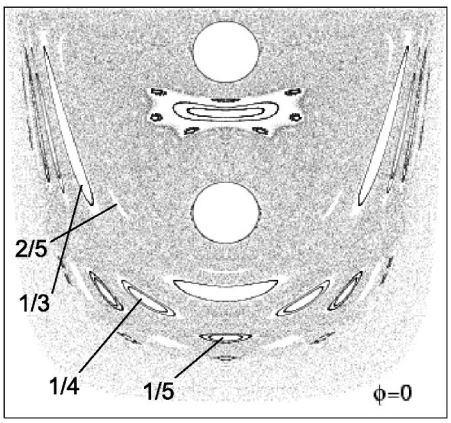

FIG. 13. The Poincaré section for the two-particle problem with $r=0.075$.

ACKNOWLEDGMENT

This work was supported by the Dutch Polymer Institute, Project No. 161.

APPENDIX: SYMMETRIES IN THE SINGLE-PARTICLE PROBLEM

Here we derive the symmetry in the Poincaré map [Eq. (30)] from the symmetry in the velocity field [Eq. (28)] for the single-particle problem. The procedures adopted here are similar to those used in Hwang *et al.*[15,16] for the steady three-dimensional open flow system with the spatially periodic perturbation.

For the notational convenience, let us define a phase-inversive reflection symmetry transformation $S_{x\phi}$ such that

$$S_{x\phi}:(x,y,\phi)\rightarrow(1-x,y,2\pi-\phi). \tag{A1}$$

$S_{x\phi}S_{x\phi}=I$, with the identity transformation I. Then the symmetry of the velocity field [Eq. (28)] can be rewritten as

$$u(\boldsymbol{p})=u(S_{x\phi}\boldsymbol{p}),\quad v(\boldsymbol{p})=-v(S_{x\phi}\boldsymbol{p}) \tag{A2}$$

at the fluid material point $\boldsymbol{p}=(x,y,\phi)$ in $\mathbb{R}^2\times S$. Now consider the motion of a fluid particle $\boldsymbol{p}$ in the flow. First, let us define infinitesimal forward time integration F and backward time integration B such that

$$F\boldsymbol{p}=(x+u\,\delta t,y+v\,\delta t,\phi+\omega\delta t), \tag{A3}$$

$$B\boldsymbol{p}=(x-u\,\delta t,y-v\,\delta t,\phi-\omega\delta t). \tag{A4}$$

Then

$$\begin{aligned}FS_{x\phi}\boldsymbol{p}&=(1-x+u\,\delta t,y-v\,\delta t,2\pi-\phi+\omega\delta t),\\&=S_{x\phi}B\boldsymbol{p}.\end{aligned} \tag{A5}$$

Therefore, the infinitesimal particle motion satisfies the following symmetry:

$$B\boldsymbol{p}=S_{x\phi}FS_{x\phi}\boldsymbol{p}. \tag{A6}$$

Moreover, by applying successive application, this symmetry holds also for finite time step,

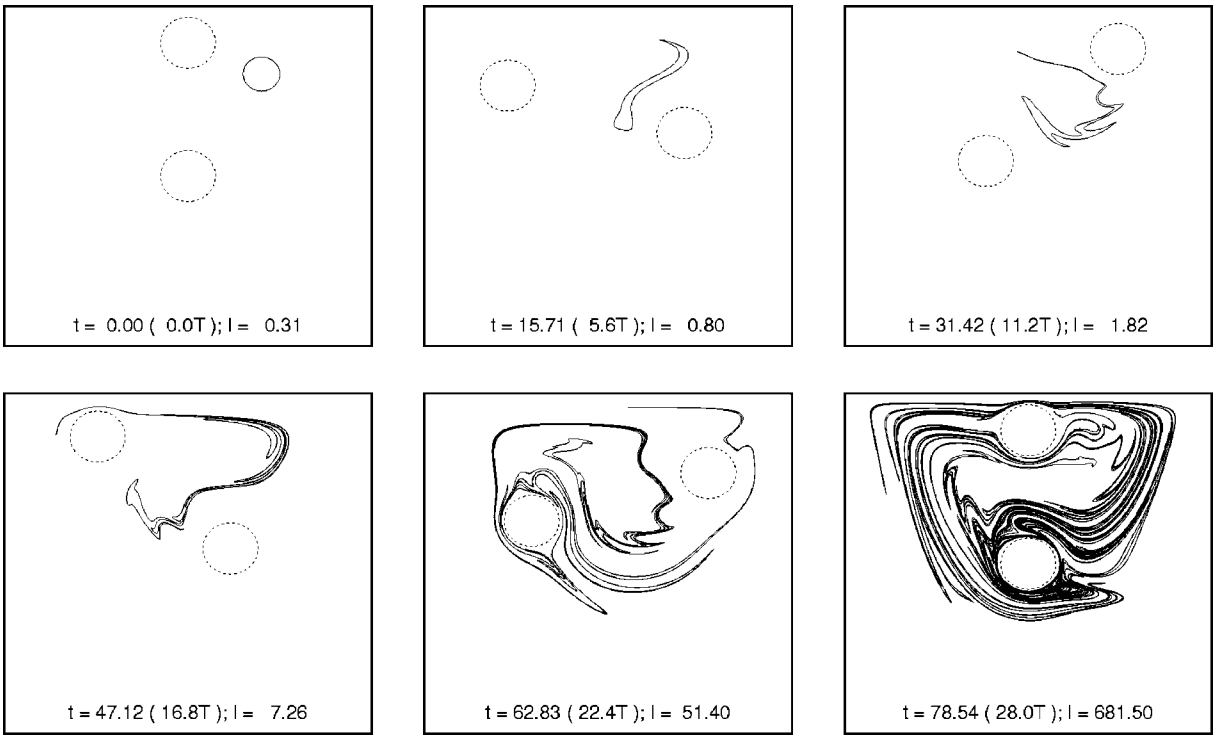

FIG. 14. The six consecutive deformation patterns of a circular fluid blob in the two-particle problem with $r=0.075$ for 28 periods with interval $5.6T$ along with length stretch l. The particles and the fluid blob are denoted by the dotted and solid lines, respectively.

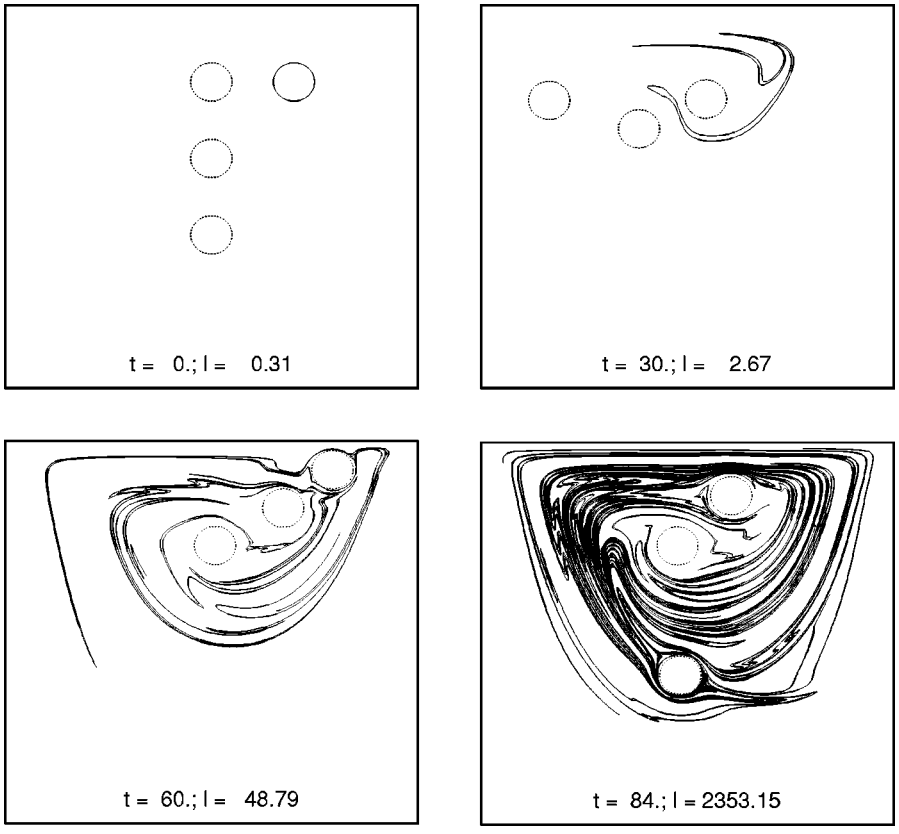

FIG. 15. The consecutive deformation patterns of a fluid blob for the three-particle problem with $r=0.05$. The particles and the fluid blob are denoted by the dotted and solid lines, respectively.

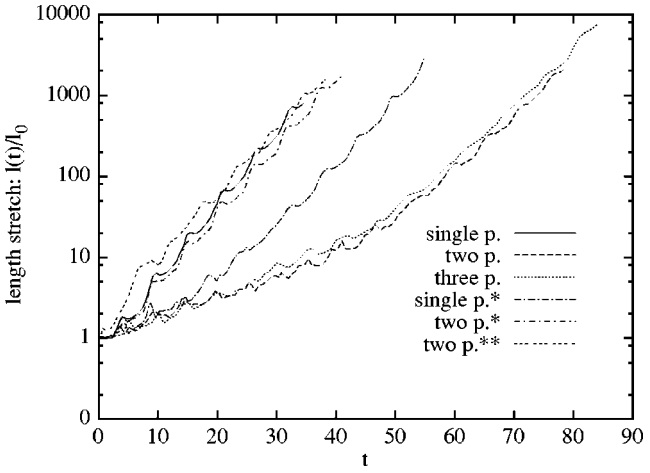

FIG. 16. The length stretch of the initially circular material lines for the single-, two-, and three-particle problems. The result is scaled by the initial length l_0.

$$B_n \cdots B_1 \boldsymbol{p} = S_{x\phi} F_n S_{x\phi} \cdots S_{x\phi} F_1 S_{x\phi} \boldsymbol{p} = S_{x\phi}(F_n \cdots F_1) S_{x\phi} \boldsymbol{p} \quad \text{for all integer } n. \tag{A7}$$

The motion of the fluid particle in the physical space $\mathbb{R}^2$ can be represented by the flow $\boldsymbol{x}(t)$ using the map φ such that

$$\varphi: \mathbb{R}^2 \to \mathbb{R}^2, \quad \boldsymbol{x}(t) = \varphi_{\phi(t_0)}^{\phi(t)}(\boldsymbol{x}(t_0)), \quad t > t_0. \tag{A8}$$

Using the two-dimensional reflection symmetry S in Eq. (29), the time-reversal backward (not inverse) flow, denoted by $\tilde{\varphi}$, can be written as

$$\tilde{\varphi}_{-s}^{-r} = S \varphi_s^r S. \tag{A9}$$

The map φ (or $\tilde{\varphi}$) commutes with 2π, i.e.,

$$(\varphi_0^{2\pi})^n = \varphi_0^{2\pi n}, \quad (\tilde{\varphi}_0^{-2\pi})^n = \tilde{\varphi}_0^{-2\pi n}. \tag{A10}$$

We choose the commutative two-dimensional map as the Poincaré map,

$$P_{\phi_0} \equiv \varphi_{\phi_0}^{2\pi+\phi_0}. \tag{A11}$$

Then the nth iterate of P_{ϕ_0} and its inverse can be written as

$$P_{\phi_0}^n = \varphi_{\phi_0}^{2n\pi+\phi_0}, \quad P_{\phi_0}^{-n} = \tilde{\varphi}_{\phi_0}^{-2n\pi+\phi_0}. \tag{A12}$$

Using Eqs. (A8) with (A12), we get the symmetry of the Poincaré map [Eq. (30)] as follows:

$$P_{2\pi-\phi_0}^{-n} = S P_{\phi_0}^n S. \tag{A13}$$

[1] M. Marić and C. W. Macosko, "Improving polymer blend dispersion in mini-mixers," Polym. Eng. Sci. **41**, 118 (2001).
[2] W. L. Chien, H. Rising, and J. M. Ottino, "Laminar mixing and chaotic mixing in several cavity flows," J. Fluid Mech. **170**, 355 (1986).
[3] J. M. Ottino, *The Kinematics of Mixing: Stretching, Chaos and Transport* (Cambridge University Press, Cambridge, 1999).
[4] H. Aref, "Stirring by chaotic advection," J. Fluid Mech. **143**, 1 (1984).
[5] S. C. Jana, M. Tjahjadi, and J. M. Ottino, "Chaotic mixing of viscous fluids by periodic changes in geometry: baffled cavity flow," AIChE J. **40**, 1769 (1994).
[6] P. D. Anderson, O. S. Galaktionov, G. W. M. Peters, and H. E. H. Meijer, "Chaotic fluid mixing in non-quasi-static cavity flows," Int. J. Heat Fluid Flow **21**, 176 (2000).
[7] A. Vikhansky, "Chaotic advection of finite-size bodies in a cavity flow," Phys. Fluids **15**, 1830 (2003).
[8] C. R. Robertson and A. Acrivos, "Low Reynolds number shear flow past a rotating circular cylinder. Part 1. Momentum transfer," J. Fluid Mech. **40**, 685 (1970).
[9] W. R. Hwang, M. A. Hulsen, and H. E. H. Meijer, "Direct simulation of particle suspensions in sliding biperiodic frames," J. Comput. Phys. **194**, 742 (2004).
[10] C. S. Peskin, "Flow patterns around heart valves: A numerical method," J. Comput. Phys. **10**, 252 (1972).
[11] R. Glowinski, T.-W. Pan, T. I. Hesla, and D. D. Joseph, "A distributed Lagrangian multiplier/fictitious domain method for particulate flows," Int. J. Multiphase Flow **25**, 755 (1999).
[12] F. P. T. Baaijens, "A fictitious domain/mortar element method for fluid-structure interaction," Int. J. Numer. Methods Fluids **35**, 743 (2001).
[13] HSL, A collection of Fortran codes for large scale scientific computation, 2002. http://www.numerical.rl.ac.uk/hsl
[14] O. S. Galaktionov, P. D. Anderson, G. W. M. Peters, and F. N. van de Vosse, "An adaptive front tracking technique for three-dimensional transient flows," Int. J. Numer. Methods Fluids **32**, 201 (2000).
[15] W. R. Hwang and T. H. Kwon, "Chaotic volumetric transports in a single-screw extrusion process," Polym. Eng. Sci. **43**, 783 (2003).
[16] W. R. Hwang, K. W. Kang, and T. H. Kwon, "Dynamical systems of pin mixers for single-screw extruders," AIChE J. **50**, 1372 (2004).
[17] P. D. Anderson, "Computational analysis of distributive mixing," Ph.D. thesis, Eindhoven University of Technology, 1999.
[18] W. R. Hwang, M. A. Hulsen, and H. E. H. Meijer, "Direct simulations of particle suspensions in a viscoelastic fluid in sliding bi-periodic frames," J. Non-Newtonian Fluid Mech. **121**, 15 (2004).